Journal of Visualization, Vol. 7, No. 2 (2004) 159-166

Tomographic Reconstruction of Asymmetric Soot Structure from Multi-angular Scanning

Lee, S. M. *[1], Hwang, J. Y. *[2] and Chung, S. H. *[2]

*1 Emission Control Group, Korea Institute of Machinery and Materials, Daejeon, 305-343, Korea.
*2 School of Mechanical and Aerospace Engineering, Seoul National University, Seoul, 151-742, Korea.
E-mail: shchung@snu.ac.kr

Received 1 May 2003
Revised 6 August 2003

Abstract : A tomographic deconvolution technique using the Fourier transformation has been applied for the reconstruction of asymmetric soot structure. Local soot volume fraction distribution can be identified from line-of-sight integrated data using light extinction measurements with multi-angular scanning. A peak-following interpolation technique was adopted to effectively increase the number of scanning angles. The results showed that the peak-following interpolation has improved the accuracy of reconstruction compared to the arithmetic interpolation in determining the local soot volume fraction. The measurement from a laser-induced incandescence technique substantiated the validity of the reconstruction technique.

Keywords : Soot, Tomography, Peak-following interpolation, Light extinction

1. Introduction

Multiple fuel jets have been utilized in practical combustors in order for flame stabilization and higher thermal load. This can cause an interaction among flames accompanying significant variations in flame structure and combustion characteristics (Roper, 1979). When a flame is merged with a neighboring flame due to flame interaction, the soot zones become complicated to have an asymmetric structure.

The Mie scattering technique has been utilized to quantify the volume fraction of small particles laden in a flow field. Especially, a light extinction technique using a laser has been adopted frequently to measure the volume fraction of soot particles. One of the disadvantages in the technique is that it requires a reconstruction process to determine spatially resolved information, because the light extinction represents the line-of-sight integrated information along the linear path of light passing through a test section.

The reconstruction for an axisymmetric flow field, where the only variation of particle distribution is in the radial coordinate, is relatively simple, since local information can be obtained by scanning a laser beam along only one angular orientation and by employing simple reconstruction techniques such as the Abel transformation or the onion peeling method. For an asymmetric case, however, the output varies with the angular orientation of scanning. Thus, measurements should be performed over several different angular orientations and the reconstruction needs rather complicated tomographic algorithms such as the Fourier transforms (Goulard et al., 1980). In such a

case, measurements require many scanning angles to improve accuracy since reconstructed result is sensitive to the number of scanning angles.

Considering that even a multi-point scanning at a given angular orientation is time consuming, the increase in the number of scanning angles is practically limited in most situations. Thus, the minimization of scanning angles while maintaining the accuracy of reconstruction is one of the key interests in light extinction measurements for asymmetric flames. In this regard, an interpolation method to effectively increase the number of projections from the limited number of actually measured extinction data is proposed and tested in the present study.

2. Experiment

The apparatus consisted of a burner, a light extinction/scattering setup, and a laser-induced incandescence (LII) measurement system. The burner has two fuel nozzles aligned in parallel having 10.7 mm i.d. with the separation distance between the nozzles of 15.2 mm. These two nozzles are imbedded into an outer oxidizer nozzle with 100 mm i.d. Air is supplied to the outer nozzle passing through glass beads and a honeycomb to attain uniform flow condition. The fuel was commercially pure grade (> 99.5 %) propane. The exit velocities of fuel and air were 1.8 cm/s and 17 cm/s, respectively. The flame stabilized in this burner formed a connected flame surface having an asymmetric structure, as shown in Fig. 1.

Fig. 1. Flame photograph in double coaxial burner.

The light extinction/scattering setup (Hwang et al., 1998) utilizes a He-Ne laser (Uniphase, 1135) with 13 mW at 632.8 nm and an Ar-ion laser (Coherent, Innova 70) with 0.5 W at 514.5 nm for extinction and scattering measurements of soot particles, respectively (Fig. 2). A photodiode monitored the extinction intensity. The scattering signals were measured by a photomultiplier tube (Hamamatsu, R928) at the right angle through a narrow band-pass filter (514.5 nm, 1 nm FWHM). The measured signals were processed by a lock-in-amplifier (Stanford Research, SR530) to enhance signal-to-noise ratio. Both the angular orientation and horizontal location of the incident laser beam relative to the flame were varied by a 3-D positioning system which can move the burner vertically, horizontally, and rotationally with the resolution of 0.1 mm, 0.25 mm, and 0.24°, respectively. There was 5 s detection delay after each movement for flow stabilization.

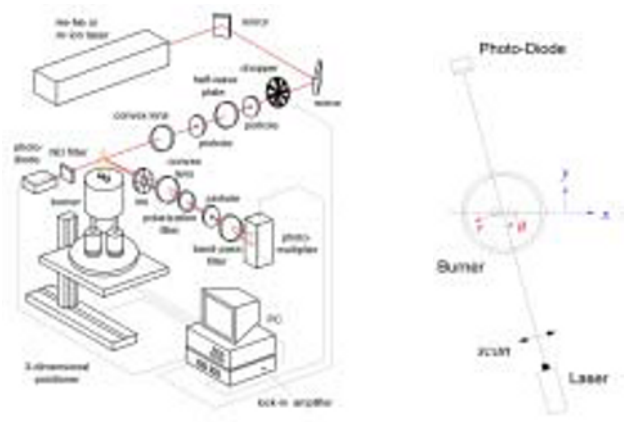

Fig. 2. Schematic of experimental setup for light extinction and scattering measurements and coordinate system.

In the LII experiment, a frequency-doubled 532 nm Nd:YAG laser (Continuum, Powerlite 8000) beam passing through a set of cylindrical lenses formed a sheet beam. LII images were taken at the right angle by an ICCD camera (Princeton Instrument, EEV 02-06) through a 400 nm narrow bandpass filter (FWHM 10 nm) to minimize the noise from scattering and fluorescence.

Tomographic Reconstruction

The principle of a tomographic reconstruction technique is briefly explained here. Let (x, y)

represent the location in the Cartesian coordinate and (r,θ) in the circular coordinate (Fig. 2). Then, the measured projection data $g(r,\theta)$ and the spatial volume fraction data $f(x,y)$ can be related by the following line-of-sight integrals in the light extinction measurement

$$g(r,\theta) = \int_{-\infty}^{\infty} f(x,y)ds = \int_{-\infty}^{\infty} K_{ext}(x,y)ds = -\ln\left[I(r,\theta)/I_0\right] \tag{1}$$

where s indicates the laser beam direction, K_{ext} is the extinction coefficient, I is the intensity of laser light, and the subscript 0 indicates the initial state.

By taking a series of Fourier transformation with the central slice theorem, the spatially resolved volume fraction can be expressed as the following discrete summation,

$$f(x,y) = \frac{1}{MN}\sum_{j=1}^{N}\sum_{k=1}^{M} g(r_k,\theta_j)\,\varphi(x\cos\theta_j + y\sin\theta_j - r_k) \tag{2}$$

where M and N represent the number of horizontal scans and the number of projection angles, respectively, and $\theta_j = (j-1)\pi/N$, $r_k = -1+2k/M$. For the filter function φ, the Shepp and Logan function was adopted. Details of the procedure can be found in Lee et al. (1997).

If soot particles are assumed sufficiently small compared to the laser wavelength, the soot volume fraction ϕ can be approximated as follows (Dobbins et al. 1984)

$$\phi = \frac{\pi}{6} N D_{30}^3 = \frac{\lambda K_{ext}}{6\pi E(\tilde{m})} \tag{3}$$

where $\tilde{m}$ is the refractive index of soot particles, known to be $1.89 - 0.48i$ when using He-Ne laser with 632.8 nm. The extinction coefficient $E(\tilde{m})$ is $E(\tilde{m}) = \mathrm{Im}\left\{(\tilde{m}^2-1)/(\tilde{m}^2+1)\right\}$.

3. Results and Discussion

The distribution of line-of-sight extinction data at various projection angles at the height of h = 25 mm above the nozzle is shown in Fig. 3(a). The burner was rotated at 3.6° interval to obtain the equiangular projections with N = 50. Each projection scans horizontally with M = 61 measurements with 0.4 mm interval, thus the total scan range is 24 mm. The vertical axis represents $-\ln(I/I_0)$, which is the integration of extinction coefficient K_{ext} along the laser beam path in Eq. (1). Note that an angular scan at a specified height requires about 10 minutes.

The local values of $K_{ext}(x,y)$ can be calculated by applying Eq. (2) from the measured data. The reconstruction result of the local soot volume fraction, shown in Fig. 3(b), demonstrates that the soot particles are concentrated near the flame surface having a peanut-shape. This distribution is due to the interaction of a typical circular distribution of soot in a single nozzle diffusion flame, which is interacted with the neighboring circular distribution when the two nozzles are very close.

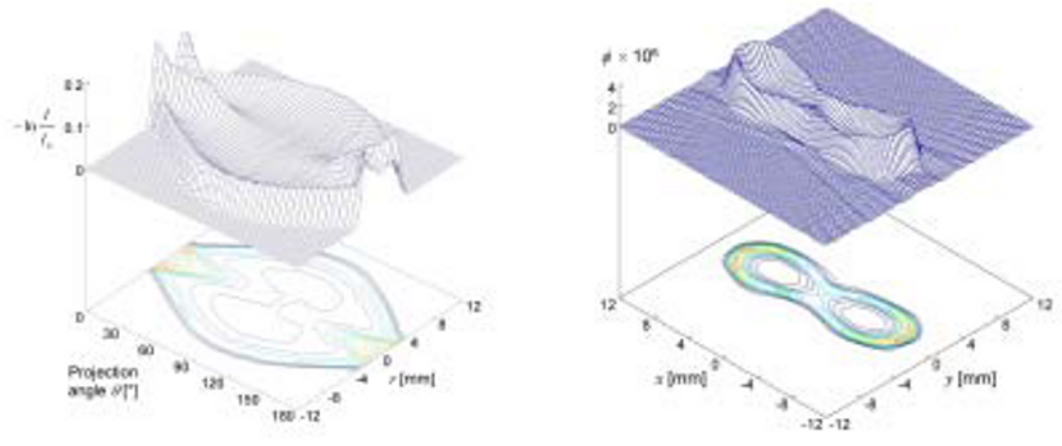

(a) (b)

Fig. 3. Distribution of (a) measured extinction data and (b) reconstructed soot volume fraction at h = 25mm for M = 61 and N = 50.

If the number of projection angles N decreases, the errors associated with the reconstruction procedure will be amplified. Figure 4 shows the reconstruction results for N = 10, and 25, whose extinction data are selected from the N = 50 data. One of the interesting features when adopting small N is that the results demonstrate appreciable wavy noise, especially outside the flame region. This seems to be pertinent to the discrete summation in the inverse Fourier transformation.

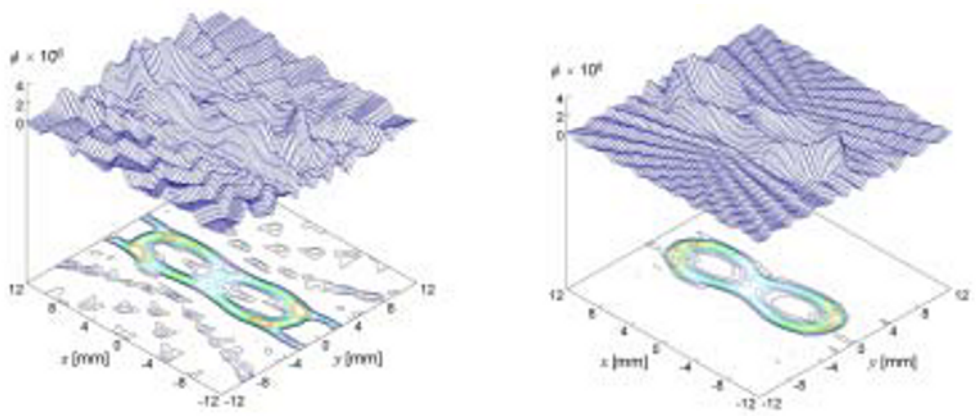

(a) (b)

Fig. 4. Distribution of soot volume fraction at h = 25 mm for (a) N = 10 and (b) N = 25.

To quantify accuracy, the following reconstruction error ε is introduced (Anderson, 1989)

$$\varepsilon = \left\{ \sum_{i=1}^{I} \sum_{j=1}^{J} \left| \hat{f}_{ij} - f_{ij} \right|^2 \right\} \Big/ \left\{ \sum_{i=1}^{I} \sum_{j=1}^{J} \left| f_{ij} - \bar{f}_{ij} \right|^2 \right\} \tag{4}$$

where $\hat{f}_{ij}$ is the calculated value, f_{ij} is the real value, and $\bar{f}_{ij}$ is the mean value of f_{ij}. Here, the value of f_{ij} are replaced with the reconstruction data for N = 50. Thus, ε indicates the relative deviation from the reconstruction results from N = 50. The reconstruction error ε is found to be 0.0509, 0.645, and 2.31 for N = 25, 10, and 5, respectively. The result demonstrates that the reconstruction accuracy is highly dependent on the number of projection angles.

A large number of projections with high spatial resolution are required for the accurate reconstruction of soot distributions using the inverse Fourier transform from the line-of-sight information. This is partly because soot particles are concentrated locally near the flame front. Since multi-point and multi-angular scanning is time consuming, it is preferable to extract relatively accurate data from limited number of projections. One method is to effectively increase the number of projection angles from measured data by adopting a suitable interpolation.

In this regard, a simple interpolation through numerical averaging has been considered first. The arithmetic mean method, however, could cause appreciable errors because of stiffness in the extinction data and the variation of peak locations according to projection angle as shown in Fig. 3(a). A peak-following interpolation technique has been adopted previously to resolve this problem for a twin-jet spray, where the data have only two peak trajectories (Lee et al., 1997). The present data show multiple peaks depending on projection angles, whose number varies from 2 to 4 as shown in Fig. 5(a). Thus, to accommodate the multi-peak characteristics, the present interpolation is performed sectionally at each region surrounded by peaks, as is marked (A, B, and C) in the figure.

Figure 5(b) shows the schematic of the peak-following interpolation technique. Here, θ_i and θ_{i+1} are the measured projection angles and $\theta_{i+1/2}$ is the intermediate angle whose data are to be interpolated. Thus, the data on the rectangular grid points at $\theta_{i+1/2}$ are to be determined from the measured data on the grid points at θ_i and θ_{i+1}. First, the peak locations at $\theta_{i+1/2}$ (●) can be determined from those at θ_i and θ_{i+1} (○) (①). Then, from the relative position of the grid points at $\theta_{i+1/2}$ (■), the corresponding positions at θ_i and θ_{i+1} (□) can be determined. An interpolation between measured data

can estimate the extinction data for these points (②). Finally, the extinction data at $\theta_{i+1/2}$ (■) can be calculated from the interpolation (③).

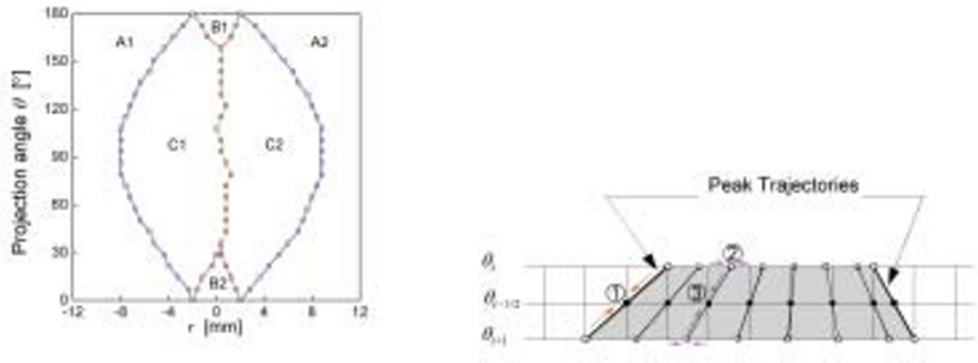

(a) (b)

Fig. 5. Schematic of (a) peak trajectories at h = 25 mm and (b) a peak-following interpolation method.

The interpolated extinction data are compared with the base data with N = 50 in Fig. 6. The peak-following interpolation is performed at the respective 6 regions marked in Fig. 5(a). The number of scanning angles is doubled to 50 from the measured data with N = 25 through the interpolation technique. For the comparison, the arithmetic averaging is also performed by interpolating data at the rectangular grid points (b). The results shown in Fig. 6(b) demonstrate that

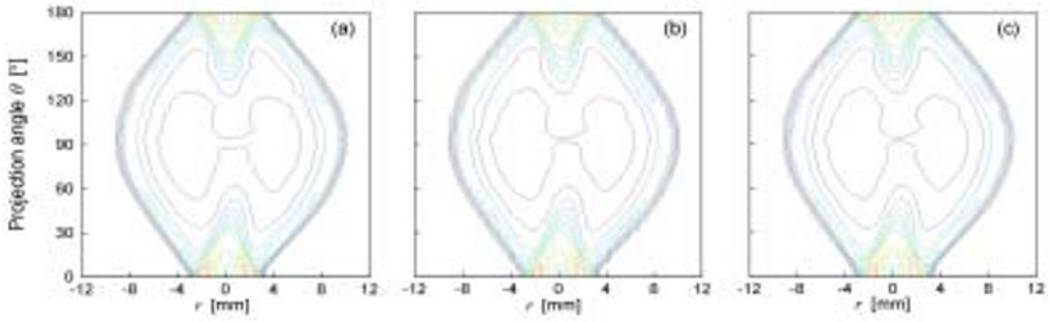

Fig. 6. Comparison of interpolated data; (a) base data for N = 50, (b) interpolated data with arithmetic averaging from N = 25 data, and (c) peak-following interpolation from N = 25 data.

the data with the arithmetic interpolation exhibit wriggling especially near the peak regions, which could deteriorate the reconstruction accuracy. In the case of the peak-following interpolation, the data are smoother and closely reproduce the original data. To further illustrate the effectiveness of the peak-following interpolation, Fig. 7 represents the interpolated data at the projection angle of 162.0°. The arithmetic averaging results in the significant decrease in the peak values as well as the shift of peak locations, while the peak-following interpolation leads to satisfactory agreement with the base data.

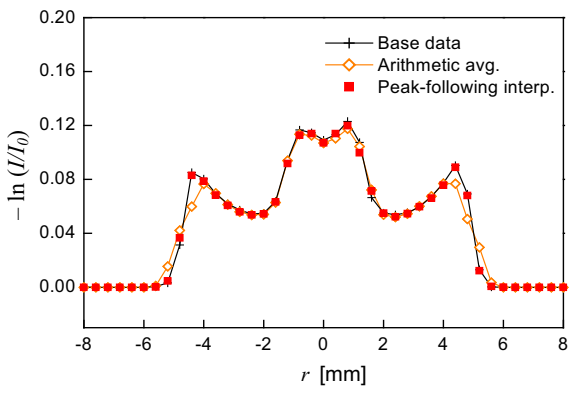

Fig. 7. Comparison of interpolated extinction data with measured data at θ = 162.0°.

Reconstruction results calculated after effectively increasing the number of projection angles through the arithmetic and peak-following interpolations are shown in Figs. 8 and 9, respectively. Here, N = 10 × 5, for example, indicates that

the measured data with N= 10 are multiplied to have N= 50 through the interpolation. For N= 10 × 5 cases, the peak-following interpolation shows significant improvement over the arithmetic interpolation, especially the sharpness of the peaks and the wavy noise outside the peanut-shaped soot region. Meanwhile, for both of the N= 25 × 2 cases the reconstruction results seem to reasonably represent the base reconstruction results shown in Fig. 3(b).

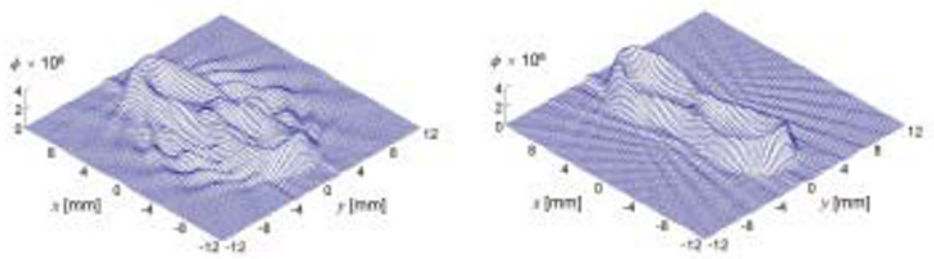

(a) (b)

Fig. 8. Reconstructed soot volume fraction with arithmetic averaging for (a) N = 10 × 5 and (b) 25 × 2.

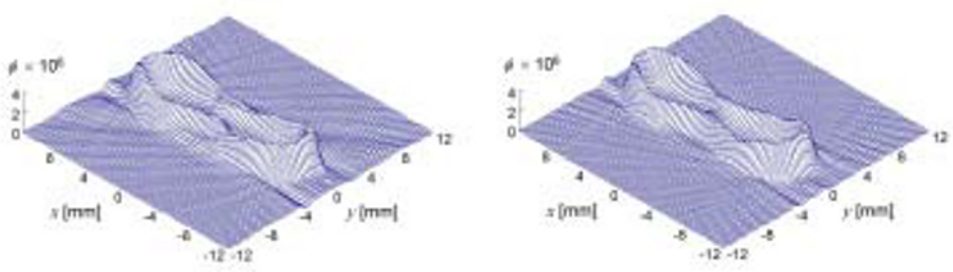

(a) (b)

Fig. 9. Reconstructed soot volume fraction with peak-following interpolation for (a) N = 10 × 5 and (b) 25 × 2.

The reconstruction errors by using the limited number of the measured data with N= 10 and 25 are compared for the case without having interpolation and with the interpolations. Here, the N value after interpolation is 50 for all the interpolated cases. The reconstruction errors are listed in Table 1.

Table 1. Comparison of reconstruction errors ε.

Measured N	10	25
W/o interpolation	0.645	0.0509
Arithmetic	0.170	0.0147
Peak-following	0.0627	0.00787

Compared to the arithmetic interpolation, the peak-following interpolation reduces the errors appreciably, although it is difficult to be distinguished in the graphical representations for the N= 25 × 2 cases. Meanwhile, a test also has been performed for the case of N = 50 × 2, confirming the accuracy of N= 50 data.

One point to note is that the wavy noise is drastically reduced by simply increasing the number of projection angles through interpolations as demonstrated in Figs. 8 and 9. To exclude this wavy noise effect in the error calculation, the reconstruction data having larger than 5 % of the maximum soot volume fraction are analyzed. This error $\varepsilon_{>5\%}$ is listed in Table 2.

Table 2. Comparison of reconstruction errors $\varepsilon_{>5\%}$.

Measured N	10	25
W/o interpolation	0.421	0.0173
Arithmetic	0.278	0.0231
Peak-following	0.0910	0.0115

Note that the errors $\varepsilon_{>5\%}$ for the arithmetic interpolation become comparable to the errors of

the reconstruction data without having interpolations. Especially for N= 25, the deteriorating effect by the improper choice of interpolation method is amplified such that $\varepsilon_{>5\%}$ for the arithmetic interpolation is even higher than the case without having interpolation. This result substantiates the usefulness of the peak-following interpolation technique.

The planar image of LII signal is obtained and compared with the reconstructed result. The intensity of LII signal is known to be reasonably proportional to soot volume fraction. Figure 10 shows the LII image at the vertical cross-section of the flame along the line joining the two axes of the nozzles (a) and the distribution of soot volume fraction obtained by the height-by-height reconstruction of light extinction (b), and the distribution of the soot particle size obtained from laser light scattering and extinction measurements (c). The LII signals are found to agree well with the reconstruction results in the soot region where particle sizes are relatively large. However, in the incipient soot region of the height 20 < h < 25 mm near the center line where particle sizes are small, the LII measurement underestimates the local soot volume fraction compared to those measured by the light extinction technique. This can be attributed to nonlinear aspects of LII signal due to the characteristics of vaporization and cooling of the soot particles, which depend on the size of soot particles (Vander Wal, 1996). Meanwhile, the LII technique has advantages in acquiring the distribution of soot volume fraction since the technique does not require reconstruction. However, the technique has the problem in quantification by the nonlinearity in contrast to the light extinction technique.

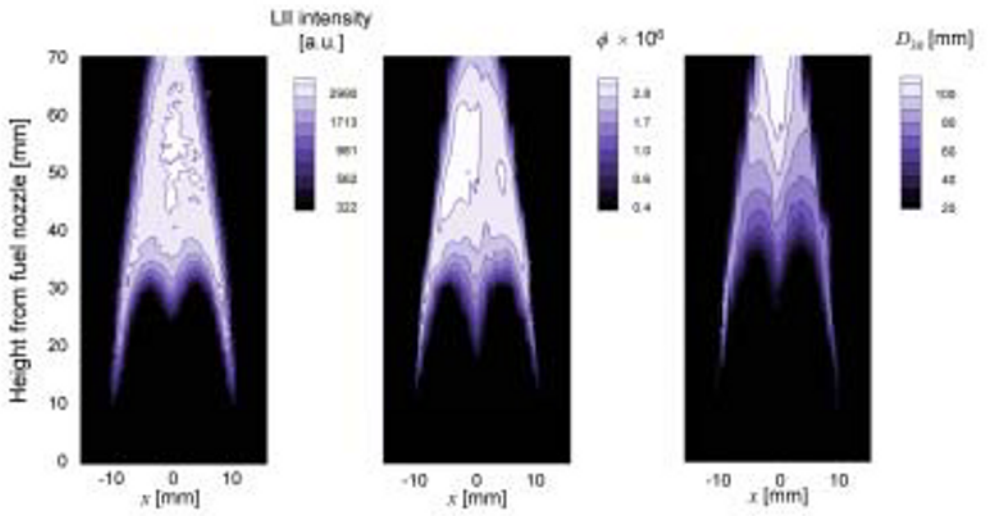

(a) (b) (c)

Fig. 10. Distribution of soot particles along vertical cross section; (a) LII signals, (b) soot volume fraction, and (c) volume-averaged diameter.

4. Concluding Remarks

The line-of-sight extinction measurement data of soot particles have been successfully transformed to reconstruct spatially resolved soot volume fraction by using the convolution Fourier transforms. The accuracy of the tomographic reconstruction depends sensitively on the number of projections due to the localized soot distribution near the flame front. Since the scanning of extinction data is time-consuming, it is necessary to effectively increase the number of projections through interpolation. The peak-following interpolation technique by dividing interpolation regions from peak trajectories has been applied and compared with the arithmetic interpolation technique. The results demonstrate the effectiveness of the peak-following interpolation technique. Comparison with LII images substantiated the validity of the reconstruction technique.

References

Anderson, A. H., IEEE Transaction on Medical Imaging, 8 (1989), 50-55.
Dobbins, R. A., Santoro, R. J. and Semerijian, H. G., Progress in Astronautics and Aeronautics, 92 (1984), 208-237.
Goulard, R. and Emmerman, P. J., Inverse Scattering Problems in Optics, H. P. Baltes, Ed., Springer Verlang, Berlin. (1980), 215-235.
Hwang, J. Y., Lee, W., Kang, H. G. and Chung, S. H., Combustion and Flame, 114 (1998), 370-380.
Lee, C. H. and Chung, S. H., Atomization and Sprays, 7(1997), 183-197.
Roper, F. G., Combustion and Flame, 34 (1979), 19-27.
Vander Wal, R. L., Applied Optics, 35-33 (1996), 6548-6559.

Author Profile

Lee Sang Min: He received his B.S. degree in Mechanical Engineering in 1997 and his Ph. D. degree in Mechanical Engineering in 2003 from Seoul National University. He is now a senior researcher in Korea Institute of Machinery and Materials. His research interests are laser diagnostics, soot formation, and non-thermal plasma.

Hwang Jun Young: He received his B.S. degree in Mechanical Engineering in 1993 and his Ph. D. degree in Mechanical Engineering in 1999 from Seoul National University. He is now a head researcher in CATech Inc. His research interests are laser diagnostics, soot formation, and flame synthesis.

Chung Suk Ho: He received his B.S. degree in Mechanical Engineering in 1976 from Seoul National University, and his Ph. D. degree in Mechanical Engineering in 1983 from Northwestern University. He is a professor since 1984 in the School of Mechanical Engineering, Seoul National University. His research interests cover combustion fundamentals, pollutant formation, and laser diagnostics.